

A Two-Region Diffusion Model for Current-Induced Instabilities of Step Patterns on Vicinal Si(111) Surfaces

Tong Zhao¹ and John D. Weeks^{1,2}

¹*Institute for Physical Science and Technology, University of Maryland, College Park, Maryland 20742 and*

²*Department of Chemistry and Biochemistry, University of Maryland, College Park, Maryland 20742*

(Dated: November 21, 2018)

We study current-induced step bunching and wandering instabilities with subsequent pattern formations on vicinal surfaces. A novel two-region diffusion model is developed, where we assume that there are different diffusion rates on terraces and in a small region around a step, generally arising from local differences in surface reconstruction. We determine the steady state solutions for a uniform train of straight steps, from which step bunching and in-phase wandering instabilities are deduced. The physically suggestive parameters of the two-region model are then mapped to the effective parameters in the usual sharp step models. Interestingly, a negative kinetic coefficient results when the diffusion in the step region is faster than on terraces. A consistent physical picture of current-induced instabilities on Si(111) is suggested based on the results of linear stability analysis. In this picture the step wandering instability is driven by step edge diffusion and is not of the Mullins-Sekerka type. Step bunching and wandering patterns at longer times are determined numerically by solving a set of coupled equations relating the velocity of a step to local properties of the step and its neighbors. We use a geometric representation of the step to derive a nonlinear evolution equation describing step wandering, which can explain experimental results where the peaks of the wandering steps align with the direction of the driving field.

I. INTRODUCTION

Steps on vicinal surfaces exhibit many different instabilities in the presence of non equilibrium driving forces. Of particular interest to us here are the current-induced instabilities on Si surfaces that were first discovered by Latyshev *et al.*¹ in 1989. After resistive heating of a vicinal Si(111) surface with a step-down direct current at temperature around 900°C, they observed the formation of closely packed step bunches separated by wide step-free terraces. The uniform step train remained stable on heating with a step-up current. This instability has a mysterious temperature dependence,^{2,3,4,5,6} with three temperature ranges between 830°C and 1300°C where the unstable current direction reverses.

Furthermore, recent experiments^{7,8,9} in temperature range II (about 1050°C to 1150°C) have shown that after heating for several hours with a step-down current, the initially uniform steps exhibit a novel *wandering instability* with finite wavelength in-phase sinusoidal undulations in their positions. When the current is directed at an angle to the average step direction, the undulations are continuously distorted by the field until finally all the peaks point in the direction of the field.¹⁰

These instabilities likely arise from a complex interplay between the driven diffusion of adatoms induced by the electric field \mathbf{E} and their attachment/detachment kinetics at steps, which serve as sources and sinks of adatoms. (Island formation is not important in the temperature regimes we consider.) Adatoms are believed to acquire a small effective charge z^*e , which includes both electrostatic and “wind-force” contributions arising from scattering of charge carriers, and thus experience a force $\mathbf{F} = z^*e\mathbf{E}$ that biases their diffusive motion.¹¹ Typically \mathbf{E} has a magnitude of about 5 ~ 10V/cm and z^* is of the

order of $10^{-3} - 10^{-1}$ for Si.^{4,12}

Most theoretical methods are based on a generalization of the approach taken by Burton, Cabrera and Frank (BCF),¹³ where one considers field driven diffusion of adatoms on terraces, with boundary conditions at the steps, viewed as line sources and sinks. We will generally refer to these generalized BCF models as *sharp step models*. Surface reconstruction typically seen on semiconductor surfaces clearly has important effects on the movement of adatoms on terraces and may well affect the attachment kinetics at steps. While it is relatively simple to take account of reconstruction on terrace diffusion by changing the diffusion constant, it is much less clear how it should be incorporated into the boundary conditions at the step edges.

Many different boundary conditions have been proposed, incorporating, e.g., asymmetric attachment-detachment barriers,^{14,15} periphery diffusion along a step,¹⁶ permeable steps,^{17,18} and field-dependent kinetic coefficient,²⁰ and researchers have shown that different combinations can give results that can agree with some experiments on current-induced step bunching. However, a general understanding of the physics leading to the sharp step boundary conditions and how they are affected by reconstruction and the external field is far from clear.

We discuss here a simple model incorporating the key physical features of driven diffusion and surface reconstruction. It can provide a consistent explanation of many experimental results on both Si(111) and Si(001) surfaces in terms of a few effective parameters. The model also provides a physically suggestive way of interpreting sharp step boundary conditions, showing how the effective parameters in continuum models can be related to kinetic processes on vicinal surfaces.²¹

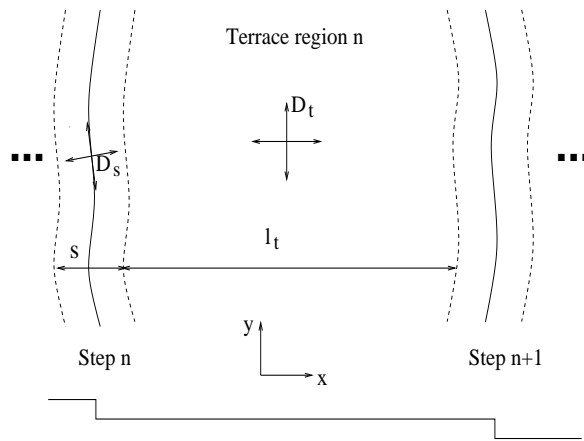


FIG. 1: The upper part of the figure shows a 2D schematic view of the vicinal surface composed of different reconstruction regions on terraces and near steps, separated by dashed lines. In this paper, we assume that the step reconstruction with a fixed width s always follows the motion of the step (solid line). The lower part of the figure shows a corresponding 1D side view that illustrates our coordinate system.

In the following, we will set up the basic two-region diffusion model and then examine the non-equilibrium steady state (NESS) solutions. Step bunching and wandering regimes are discussed, and combined to provide a coherent scenario for the complicated Si(111) electromigration experiments. A mapping to the generalized BCF model is presented next that sheds light on the sharp step boundary conditions. Finally, we study the long time and nonlinear behavior of these instabilities and find some intriguing patterns that resemble many features seen in real experiments on Si(111) surfaces. An alternate derivation of the basic equations and applications to the different instabilities seen in Si(001) surfaces is given elsewhere.²²

II. TWO-REGION DIFFUSION MODEL AND STEADY STATE SOLUTIONS

It is well known that the dangling bonds at semiconductor surfaces quite generally rearrange to form characteristic surface reconstructions. We expect a different local rearrangement of bonds in the vicinity of a step, which itself represents an additional source of dangling bonds. Clearly this reconstruction can directly influence surface mass transport and hence possible instabilities. Standard boundary conditions in the continuum sharp step model may include some effects of surface reconstruction in special cases. For example, Liu and Weeks²³ interpreted electromigration experiments in the lowest temperature regime of Si(111) using attachment/detachment limited kinetics, and argued that the attachment barriers could arise from a local reconstruction of the dangling bonds at a step edge. However, it is not clear how this picture should be modified at higher temperatures.

Steps differ fundamentally from terraces by serving as

sources and sinks for adatoms. In the classical BCF picture it was assumed that the local equilibrium concentration of adatoms at a step is maintained even in the presence of nonequilibrium driving forces. In addition the rates of various mass transport processes near steps can differ from kinetic processes on terraces, e.g., because of differences in local surface reconstructions. The kinetic coefficients in generalized BCF models try to take both features of steps into account in an effective way.

Our approach here is to consider a more detailed description where both features are treated separately in the simplest possible way. We then obtain the relevant sharp step boundary condition by an appropriate coarse-graining. To that end, we assume that an atomic step has sufficient kink sites to maintain a local equilibrium concentration of adatoms as in the classical BCF picture. Reconstruction is taken into account by assuming that the atomic step is surrounded by a *step region* where adatoms undergo effective diffusion with a diffusion constant D_s that can differ from D_t , the value found on terraces.

Here we use the simplest realization of this idea, where the reconstruction is assumed to occur fast relative to step motion, so that the step region moves with the atomic step and has a fixed width s of a few lattice spacings at a given temperature. Thus a uniform vicinal surface can be viewed as an array of repetitive two-region units, made up of the n th step region and its neighboring lower terrace region. We assume that straight steps extend along the y direction and that the step index increases in the step-down direction, defined as the positive x direction, as schematically shown in Fig. 1.

The adatoms undergo driven diffusion from the electric field. The biased diffusion flux of adatoms with density c takes the form:

$$\mathbf{J}_\alpha = -D_\alpha \nabla c_\alpha + D_\alpha \frac{\mathbf{F}}{k_B T} c_\alpha, \quad (1)$$

where $\alpha = (t, s)$ indicates the terrace or step region and D_α is the diffusion constant in the corresponding region, which here is taken to be isotropic for simplicity. We also assume that the effective charge is the same in both regions and ignore the small effects of step motion on the steady state adatom density field, since the direct field-induced adatom drift velocity is generally very much larger than the net velocity of the steps (driven by free sublimation in real experiments) even at high temperatures.²⁴

In many studies of step dynamics, because the separation of their respective time scales, it suffices to solve the diffusion problem with fixed step positions and then balance the fluxes locally at a step to determine its motion. This is often called the *quasi-stationary* approximation, and it will be adopted throughout this paper. Thus the static diffusion problem is simply

$$\nabla \cdot \mathbf{J}_\alpha = 0 \quad (2)$$

in each region, along with continuity of c and \mathbf{J} at fixed boundaries between terrace and step regions. The normal

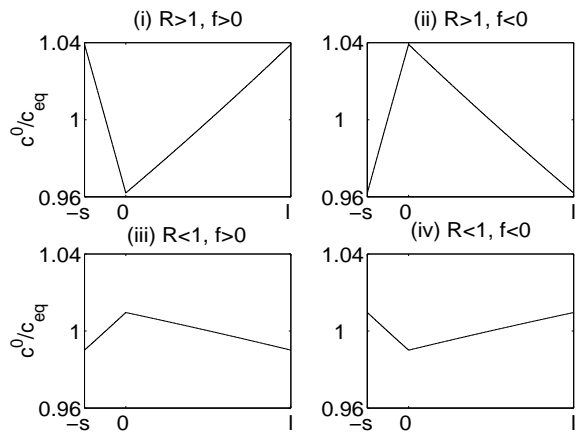


FIG. 2: Plot of concentration profiles according to Eq.(4) with model parameters. $R = 10$ for (i) and (ii), $R = 0.1$ for (iii) and (iv); $|fa| = 0.01$ in all cases.

velocity of the step region is given by mass conservation locally at an infinitesimal portion of the step region

$$v_n \Delta c = [\mathbf{J}_t^- - \mathbf{J}_t^+] \cdot \hat{n} - \int_s \partial_\tau [\mathbf{J}_s \cdot \hat{\tau}]. \quad (3)$$

Here \mathbf{J}_t^\pm denote diffusion fluxes in the front and back terraces respectively and Δc is the difference of the areal density of the two phases — the solid phase and the 2D adatom gas phase. For simplicity, we take a simple cubic lattice, so that $\Delta c \approx 1/\Omega = a^{-2}$, where a is the lattice parameter. The last term in Eq. (3) represents the contribution from diffusion flux in the step region parallel to the step, where τ denotes the arc length.

Eqs. (1-3) define the two-region diffusion model. We first consider the NESS solution corresponding to a 1D uniform step train. In this case, the step normal direction coincides with the x direction on terraces, and thus parallel or tangential diffusion in the step region plays no role here. The NESS concentration profile (denoted by a superscript '0') in a two-region unit is easily obtained by solving Eq. (2) in both regions subject to continuity of concentration and fluxes at the boundaries and is given by

$$\begin{aligned} c_s^0 &= C \left[R + \frac{(1-R)(e^{fl_t} - 1)}{e^{fl_t} - e^{-fs}} e^{fx} \right] \\ c_t^0 &= C \left[1 - \frac{(1-R)(1 - e^{-fs})}{e^{fl_t} - e^{-fs}} e^{fx} \right], \end{aligned} \quad (4)$$

Here

$$R \equiv D_t/D_s \quad (5)$$

is one of the key dimensionless parameters that describes the relative diffusion rates of adatoms on terraces and in the normal direction of step regions, $f \equiv \mathbf{F} \cdot \hat{x}/k_B T$ has a dimension of inverse length and characterizes the strength of the external field, and l_t is average terrace

width in the steady state. C is a constant to be determined shortly.

Evidently, it is the interplay between the external electric field and changes in the local diffusion rates, characterized by various combinations of the two parameters f and R , that causes the intriguing instabilities. With the electric field perpendicular to the step region, altogether there are four types of steady state adatom concentration profiles with different combinations of parameters f and R , as shown in Fig. 2. In the absence of sublimation, the concentration profiles we obtain here are completely driven by the external field. By taking the limit $f \rightarrow 0$ in Eq. (4), one should recover the equilibrium concentration (denoted as c_{eq}) on the entire surface. This fixes the constant in Eq. (4) as

$$C = c_{eq} (l_t + s) / (l_t + Rs). \quad (6)$$

Moreover, the constant flux at NESS can be written as

$$J_0(l) = D_t c_{eq} f \frac{l}{l + (R-1)s}, \quad (7)$$

where

$$l \equiv l_t + s \quad (8)$$

is the distance between the centers of two adjacent step regions in a uniform step train. Note that the NESS concentration profile of adatoms given by Eq. (4) reduces to a constant on the entire surface in presence of the field if the diffusion in the normal step direction is the same as terrace diffusion, i.e., when $R = 1$.

III. STEP BUNCHING AND WANDERING INSTABILITIES

In this section, we study the stability of the NESS solutions. In particular, the physical origins of both step bunching and wandering instabilities are qualitatively discussed.

A. Step Bunching Instability

A common feature of all NESS profiles shown in Fig. 2 is that adatom concentration gradients build up in both terrace and step regions. Under experimentally relevant conditions the field is sufficiently weak that $fs < fl_t \ll 1$ and *linear* concentration (or chemical potential) gradients form. It is then easy to see that the local equilibrium boundary condition $c = c_{eq}$ in the center of the step region holds automatically by symmetry. In the qualitative picture of step bunching discussed by Liu and Weeks,²³ a positive terrace concentration gradient (induced in their model by a step-down current with an attachment barrier at a sharp step edge) leads to step bunching. The

steady state profile they analyzed leading to step bunching in temperature regime I is very similar to case (i) in Fig. 2. This corresponds in the two-region model to a step-down field with slower diffusion in the step region, in agreement with an intuitive picture of a step barrier.

Moreover, it is clear that profile (iv) is qualitatively the same as (i). Hence we expect that the steady state (iv), corresponding to *faster* diffusion in the step region with a *step-up* field, also undergoes a bunching instability. A hopping model with these features was studied by Suga *et al.*²⁰ by computer simulations, and indeed they observed a bunching instability.

To understand the bunching of straight steps it is useful to consider a 1D version of Eq. (3):

$$v_n = \Omega [J_0(l_{n-1}) - J_0(l_n)], \quad (9)$$

where the 1D flux J_0 as given by Eq. (7) now depends on the local terrace widths. Consider a small deviation $\delta x_n = \varepsilon_n e^{\omega_1 t}$ for n th step from the NESS, where $\varepsilon_n \equiv \varepsilon e^{in\phi}$ and ϕ is the phase between neighboring steps. Then the step will move as a result of the unbalanced fluxes induced by changing width of the terrace in front $l_n = l + \varepsilon_n (e^{i\phi} - 1)$ and back $l_{n-1} = l + \varepsilon_n (1 - e^{-i\phi})$. The amplification rate ω_1 is given by $\omega_1 = v_n/\varepsilon_n$, and substituting into Eq. (9) gives

$$\begin{aligned} \omega_1 &= -2\Omega D_s \frac{dJ_0(l)}{dl} (1 - \cos \phi) \\ &= 2\Omega D_t c_{eq}^0 \frac{f(R-1)s}{[l + (R-1)s]^2} (1 - \cos \phi). \end{aligned} \quad (10)$$

Clearly, step bunching occurs when $f(R-1) > 0$, corresponding to two different regimes discussed above, and in both cases the most unstable mode is a step pairing instability with $\phi = \pi$.

B. Step Wandering Instability

The 1D NESS concentration profiles also provide important insights into step wandering, which is essentially a 2D phenomenon. It is clear that the concentration gradient on the terraces in cases (i) and (iv) can drive a step wandering instability. The monotonically increasing terrace chemical potential tends to make a forward bulging part of a step move even faster, as was first demonstrated for vicinal surfaces by Bales and Zangwill.²⁵ This is the essence of the classic Mullins-Sekerka instability.^{26,27} However, as shown above, these same profiles lead to 1D step bunching, which tends to suppress the wandering instability. Moreover, this mechanism cannot explain the behavior in regime II of Si(111) where wandering and bunching occur for *different* current directions.

The fact that this step wandering cannot be of the Mullins-Sekerka type driven by terrace gradients suggests that it may originate from mass transport in the *step* region. Let us focus on a single 2D step region, as in Fig. 3. In this case, it is convenient to describe the step region

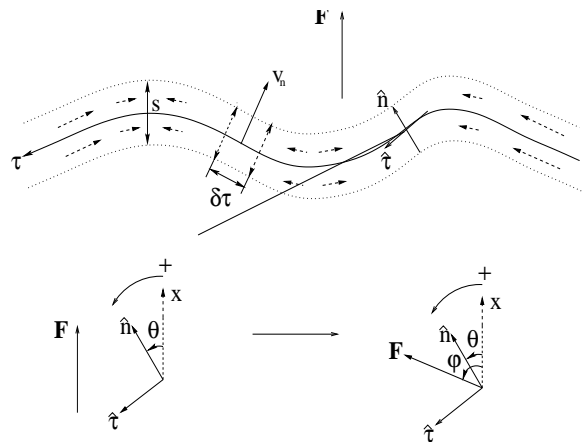


FIG. 3: A geometrical view of a single wandering step region. The dashed arrows inside the step region schematically shows the driven flux that is parallel to the step for a step-down (x direction) field. The lower right corner shows the case when the field is at an angle ϕ off the x -axis.

using curvilinear coordinates set up by the local normal and tangential directions of the step. For a long wavelength step fluctuation with wavenumber q there exists a nonzero component of the field in the tangential direction, which induces a driven flux along the step proportional to $f q^2$. For a step-down field ($f > 0$), this driven flux is destabilizing since it tends to transport mass from “valleys” to forward-bulging “hills”. On the other hand, the stabilizing flux due to the curvature relaxation is proportional to Γq^4 , where Γ is an effective capillary length in the step region. The competition between these two terms results in a finite wavelength linear instability, occurring on a length scale of order ξ , where

$$\xi \equiv \sqrt{\Gamma/|f|}. \quad (11)$$

In principle this new wandering instability could arise in cases (i) and (iii) of Fig. 2 where there is a step-down field. However step bunching also occurs for case (i). Only case (iii) with $f > 0$ and faster diffusion in the step region ($R < 1$) is free of step bunching, and thus capable of explaining experiments in Regime II of Si(111). In the next section we show that these qualitative conclusions are in agreement with a more detailed analysis based on a mapping of the two-region model to an equivalent sharp step model.

IV. MAPPING TO A GENERALIZED BCF MODEL

In this section we show how the two-region model can be used to generate the appropriate sharp step boundary conditions by a mapping to a generalized BCF model.

The general continuum boundary condition in the sharp-step model assumes small deviations from local equilibrium and introduces linear *kinetic coefficients* k_{\pm}

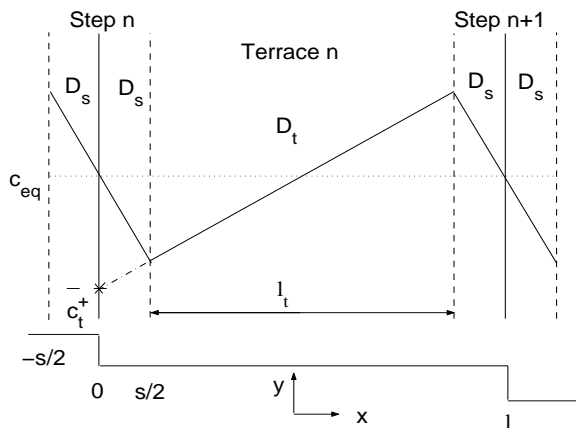


FIG. 4: Shown is a highly exaggerated profile for a downhill force and slower diffusion in the step region. Also illustrated with the dashed-dot line is the extrapolation of the terrace profile to the center of the step region, thus determining the parameter \bar{c}_t^+ in Eq. (12). The lower part of the figure gives a side view of sharp equilibrium steps and their associated step regions.

to relate \bar{c}_t^+ (or \bar{c}_t^-), the limiting lower (or upper) terrace adatom density at the step edge, to the associated terrace adatom flux into the step. To linear order in the field this gives rise to the standard sharp step boundary condition:

$$\pm D_t [\nabla c_t - f c_t]_{\pm} = k (c_t - c_{eq})_{\pm}. \quad (12)$$

Here k is the corresponding sharp step kinetic coefficient, which is symmetric in this case.

A natural way of relating the NESS solutions of the two-region model to those of sharp step model is to *extrapolate* the terrace concentration profile to the center of the step region. This corresponds to a physical coarse-graining where the step region has negligible width when compared to the terrace widths. The use of extrapolation to relate the parameters in discrete and continuum models is well known in other interface applications.²⁸ We use Eq. (4) to evaluate the gradient, and identify \bar{c}_t^{\pm} as the extrapolated value of terrace concentration at the atomic step, as illustrated in Fig. 4. Substituting into Eq. (12), to lowest order in the field we find that

$$d \equiv \frac{D_t}{k} = \frac{1}{2}(R-1)s. \quad (13)$$

Note that the terrace width l in the sharp step model is naturally related to the two-region width l_t by $l = l_t + s$, as in Eq. (8). Here d is often referred to as the attachment-detachment length.

Equation (13) gives a mapping of the parameters in the simplest two-region model to those of a generalized BCF model. When $R > 1$ (faster diffusion in the terrace region), k is positive, which leads to a bunching instability for a step-down current. When $R = 1$ (the diffusion rate is the same in both regions), k goes to infinity, which

forces \bar{c}_t^{\pm} in Eq. (12) to equal c_{eq} , corresponding to local equilibrium with no instability. When $R < 1$ (diffusion is faster in step regions than in terrace regions), k becomes *negative*, which leads to step bunching by a step-up current together with step wandering by a step-down current.

The possibility of a negative kinetic coefficient, or equivalently a negative d , was first suggested in the work of Politi and Villain,²⁹ though with no derivation or discussion of any physical consequences. Note that even though the derivation given here considers a terrace concentration profile obtained by electromigration, Eq. (13) is a general result that is independent of the field. In a related work,²² we derive sharp step boundary conditions by considering a discrete hopping model with different hopping rates in two regions but without the field, and again obtain Eq. (13).

V. LINEAR STABILITY ANALYSIS

With the mapping defined by Eq. (13), the linear stability analysis can be performed using a standard sharp step model, with parameters obtained from the physically suggestive two-region model. The general result is presented in the appendix, and here we concentrate on the resulting stability in the weak field ($fl \ll 1$) and long wavelength ($ql \ll 1$) limit. The real part of the stability function can be written as

$$\omega_r = \omega_1(f, \phi) + \omega_2(q, f, \phi), \quad (14)$$

where

$$\omega_1 = \Omega D_t c_{eq}^0 \frac{4df}{(l+2d)^2} (1 - \cos \phi), \quad (15)$$

and

$$\omega_2 = \Omega D_t c_{eq}^0 q^2 \left\{ -\Gamma \left[\frac{2(1 - \cos \phi)}{l+2d} + \left(l + \frac{s}{R} \right) q^2 \right] + f \left(\frac{2dl}{l+2d} + \frac{s}{R} \right) \right\}, \quad (16)$$

ω_1 characterizes the 1D instability and thus is independent of q . The bunching instability occurs for $df > 0$ with most unstable mode giving step pairing with $\phi = \pi$. Note that Eq. (15) is identical to Eq. (10), when Eq. (13) is used.

ω_2 characterizes 2D wandering instabilities with respect to perturbations of wavenumber q . The first term on the right hand side is stabilizing, and has its minimum value for $\phi = 0$, where it is proportional to Γq^4 and all the steps wander in phase.

The second term, proportional to the field, contains two destabilizing contributions. The first contribution, proportional to $D_t df q^2$, describes a Mullins-Sekerka or Bales-Zangwill instability induced by the terrace concentration gradient that can occur when $df > 0$.

TABLE I: Linear Stability Results

	$d > 0$ ($R > 1$)	$d < 0$ ($R < 1$)
$f > 0$	Bunching with maximum mode $\phi = \pi$ Wandering with maximum mode $\phi = 0$	Wandering with maximum mode $\phi = 0$
$f < 0$	Linearly stable	Bunching with maximum mode $\phi = \pi$

The second contribution, proportional to $D_s s f q^2$, represents an alternative mechanism for step wandering induced by field-driven periphery diffusion along the step. When $d > 0$, both mechanisms operate with a step-down current, while the step-up case is completely stable. When $d < 0$, the second mechanism can produce wandering with a step-down current, while bunching occurs for a step up current, as was discussed earlier in Sec. (III B). These stability results are summarized in Table I.

VI. IMPLICATIONS FOR SI SURFACES

Thus far, both step bunching and wandering instabilities have been analyzed in general terms based on the simple idea of two-region diffusion. Now we examine the implications for vicinal Si(111) surfaces. If we assume for concreteness that reconstruction is generally associated with slower adatom diffusion, we can give a qualitatively reasonable scenario that can account for many features of the electromigration experiments observed on Si(111).

In temperature range I, we assume there exists reconstruction in both step and terrace regions. Consistent with the analysis of Liu and Weeks, we assume that at low temperature the adatom diffusion in the reconstructed step region is slower than in the terrace region, i.e. $R > 1$, corresponding to cases (i) and (ii) in Fig. 2. A step-down current induces both step bunching and step wandering of Mullins-Sekerka type. However the wandering is likely suppressed by the bunching instability. A step-up current produces a stable uniform step train.

At higher temperatures, we expect reconstruction in step region could have a more fragile structure when compared to that in the terrace region since step atoms have more dangling bonds. Thus there could exist an intermediate temperature range where because of changes in the step reconstruction, diffusion is faster in the step region than on terraces, i.e. $R < 1$, corresponding to cases (iii) and (iv) in Fig. 2. The uniform step train now exhibits bunching with a step-up current. Wandering occurs with a step-down current, induced by driven diffusion parallel to the step. In particular, if we substitute in Eq. (11) the latest experimental values for the step stiffness,³⁰ $\tilde{\beta} = 16.3 meV/\text{\AA}$, and for the effective charge,²⁴ $z^* = 0.13$, and use a typical electric field strength of $E = 7V/cm$, the resulting wavelength is roughly given by $\lambda \simeq 2\pi\xi \sim 5\mu m$, comparable with experimental values^{7,8,9} of $6 - 9\mu m$.

In this picture, the transition between different temperature regimes is associated with local equilibrium

where $R = 1$. Conceivably, such a transition could happen again at higher temperatures, since only small changes in the relative diffusion rates can take the fundamental parameter R from less than to greater than unity and vice versa. This scenario provides a consistent interpretation of experiments in the second temperature regime and suggests more generally why there could be such a complicated temperature dependence.

VII. NONLINEAR EVOLUTION OF CURRENT-INDUCED INSTABILITIES

A. Velocity Function Formalism

To calculate the long time morphology of vicinal surfaces, effective equations relating the velocity of a step to the local terrace widths have proved to be very useful.³¹ A simple example of such a velocity function is given by Eq. (9). The *extended velocity function formalism*^{32,33} takes into account also the capillarity of steps (line tension effects) as well as step repulsions, which are needed to prevent step overhangs as the initial instabilities grow. Here we also incorporate a periphery diffusion term, the sharp step analogue of the parallel diffusion flux in the two-region model. Thus the general form of the velocity function can be written as:

$$v_n(y) = f_+(l_n; \mu_n, \mu_{n+1}) + f_-(l_{n-1}; \mu_{n-1}, \mu_n) - \partial_\tau \mathbf{J}_s \quad (17)$$

where $l_n(y)$ is the local width of terrace n that is in front of step n and $\mu_n(y)$ is the local chemical potential of the step n .

The velocity functions f_\pm contains contributions both from driven fluxes on the two neighboring terraces given by the sharp step equivalence of Eq. (9), and equilibrium relaxation terms that can be calculated in terms of the step edge chemical potentials μ_n .³⁴ The μ_n take account of both capillary effects for an individual step (using a linear approximation for the curvature) and the effects of nearest neighbor step interactions as described earlier. See Refs. 32 and 33 for detailed expressions for f_\pm and μ_n .

Numerically integrating Eq. (17), we find step bunching patterns for two parameter regimes (i) $f > 0$, $R > 1$ and (ii) $f < 0$, $R < 1$, in agreement with predictions of linear stability analysis. The bunching patterns in these two regimes are qualitatively similar, as shown in Fig. 5. In both cases, step bunches form and grow. In between the step bunches there are crossing steps traveling from

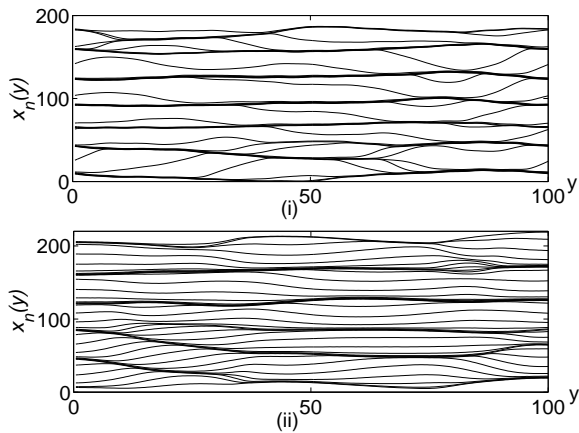


FIG. 5: A uniform step train composed of 30 steps with spacing of $l = 10$ forms step bunches at later times both for (i) $f > 0, R > 1$ and (ii) $f < 0, R < 1$.

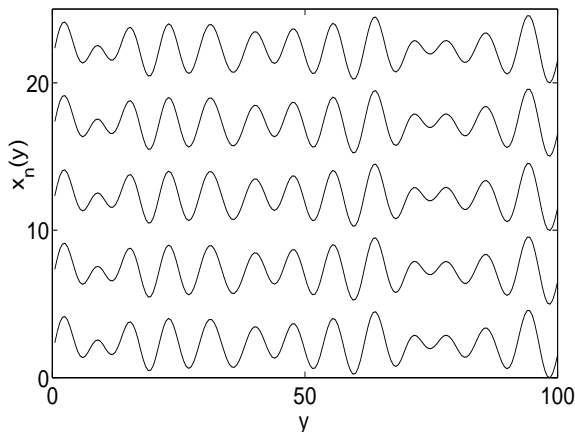


FIG. 6: A uniform step train comprised of 5 steps with spacing $l = 5$ forms in-phase wandering patterns at later times for $f > 0, R < 1$. Notice there are some defects in the pattern because the wandering wavelength is incommensurate with the finite size of our system in the y -direction.

one bunch to the other.

In-phase step wandering is also given by Eq. (17) in the regime $f > 0, R < 1$, as suggested by the previous linear stability analysis. Typical wandering patterns with model parameters are shown in Fig. 6. Even though this is known to be a linear instability, numerically we observe that it acts very like a nucleation process. The steps fluctuate randomly as if the surface were completely stable until a sinusoidal perturbation of the right wavelength forms. Once formed, these small scale sinusoidal waves propagate through effective “pulling” by capillary effects in the lateral direction and by step repulsions in the normal direction, until the entire surface is covered. This is qualitatively consistent with experimental findings on Si(111).⁹

B. Evolution of Step Wandering in a Geometric Representation

Although Eq. (17) has captured many physical features, it uses a linearized curvature approximation and cannot be trusted when the step curvature becomes large. Recent experiments show a continuous distortion of the sinusoidal wandering wave by a field directed at an angle to the step normal. We treat this problem here using a geometrical representation^{35,36} of the step, where a single curve is parameterized by intrinsic properties like its arc length τ and curvature κ .

It suffices to concentrate on a single step, since step wandering occurs in phase. Consider a geometric representation of our step region with constant width s , as in Fig. 3. The morphology of the step region is specified by the position vector $\mathbf{x}(t, \tau)$ of the atomic step in the middle, where τ can represent the arc length measured from an arbitrary origin. To follow $\mathbf{x}(t, \tau)$ at a later time we need to know the velocity of the curve

$$\frac{\partial \mathbf{x}}{\partial t} = v_n \hat{n} + v_\tau \hat{\tau}, \quad (18)$$

where \hat{n} and $\hat{\tau}$ denote normal and tangential directions as before.

A general treatment of time-dependent curvilinear coordinates³⁷ shows the equation of motion for the curve is

$$\frac{\partial \kappa}{\partial t} = - \left[\kappa^2 + \frac{\partial^2}{\partial \tau^2} \right] v_n + v_\tau \frac{\partial \kappa}{\partial \tau}, \quad (19)$$

which is subjected to the nonlocal metric constraint

$$\frac{\partial \tau}{\partial t} = v_\tau(\tau) - v_\tau(\tau = 0) + \int^\tau v_n \kappa ds'. \quad (20)$$

Interpreting τ as the arc length is arbitrary and other parameterizations can be used, since only the normal velocity of the curve is physically relevant. Following previous workers,³⁶ we take advantage of this “gauge freedom” and choose the *orthogonal gauge*, where τ is chosen at each instant of time so that the interface velocity has only a normal component ($v_\tau = 0$).

Now, we need to determine the normal velocity along the step. For simplicity, we will neglect contributions from the terrace diffusion field as well as from the normal diffusion field in the step region, since it has already been shown that the wandering instability we are interested in is induced by the biased diffusion parallel to the step. In the quasi-stationary limit, the diffusion field inside the step region is stationary for any given step position. To a good approximation, it can be taken as $c_s \simeq c_s^0 (1 + \Gamma \kappa)$, where $c_s^0 = c_{eq}^0 s$ is the adatom density per unit step length for straight steps.

Next we consider the time rate of change of the adatoms contained in an element of the step region with an infinitesimal length $\delta \tau$ that moves with velocity v_n as in Fig. 3. This balance contains contributions from

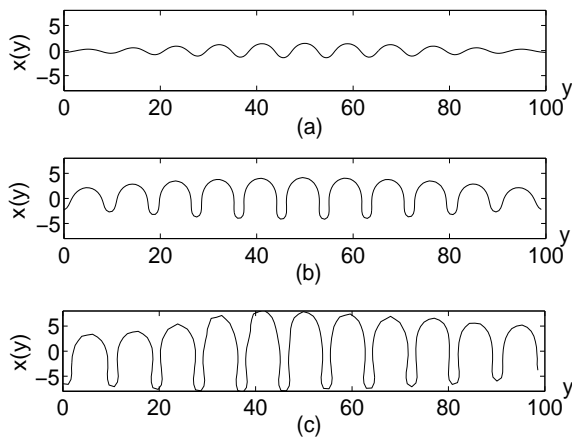


FIG. 7: Step evolution under a perpendicular electric field (a) At $t = 160$, a linear instability develops; (b) At $t = 170$, asymmetry between the peaks and valleys creates a periodic cellular structure; (c) At $t = 190$, the cellular shape is preserved but it grows in amplitude.

the motion of the step, and from the divergence of the flux parallel to the step. The latter accounts for diffusion driven both by the field and by chemical potential variations arising from changes in step curvature. We thus have

$$\left[\frac{d}{dt} (c_s \delta\tau) \right]_n = -\Omega^{-1} v_n \delta\tau - D_s \partial_\tau [f c_s \sin(\varphi - \theta)] \delta\tau + D_s \partial_\tau^2 c_s \delta\tau. \quad (21)$$

Using the exact geometrical relation $[d(\delta\tau)/dt]_n = v_n \kappa \delta\tau$, which can be understood physically as the rate at which the arc length $\delta\tau$ on a circle of radius $|\kappa^{-1}|$ changes if the circle grows only radially at rate v_n , Eq. (21) reduces to the following form

$$\frac{v_n [1 + \Omega c_s^0 (1 + \Gamma \kappa) \kappa]}{\Omega D_s c_s^0} = f \cos(\varphi - \theta) (1 + \Gamma \kappa) \kappa - f \sin(\varphi - \theta) \Gamma \partial_\tau \kappa + \Gamma \partial_\tau^2 \kappa. \quad (22)$$

Combining Eq. (22) with Eqs. (19) and (20) yields a complete description of the dynamics of a single step region in the presence of an electric field at an angle φ off the x -axis.

We first consider the special case $\varphi = 0$ where the external field is perpendicular to the average step direction (the y -axis). In Fig. 7, we show three step configurations evolving from a straight step with a small perturbation in the middle. The linear wandering instability develops first as shown in Fig. 7(a), then gradually changes into a cellular shape with the wavelength selected by the linear instability, as illustrated in Fig. 7(b). At later stages, the cellular shape grows without significant distortion or overlap, as shown in Fig. 7(c). Notice that indeed we observe numerically a long time period before the linear instability is significant.

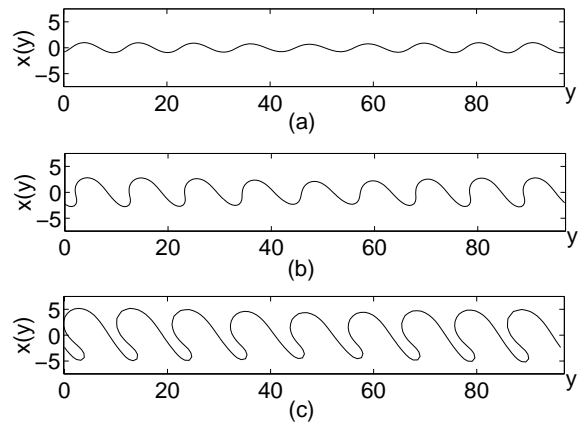


FIG. 8: Step evolution when the electric field is at an angle $\varphi = \pi/4$ from the x -axis: (a) $t = 300$, the initial instability induced by the normal component of the field; (b) $t = 315$, the peaks have begun to turn; (c) $t = 330$, all the peaks align with the direction of the field.

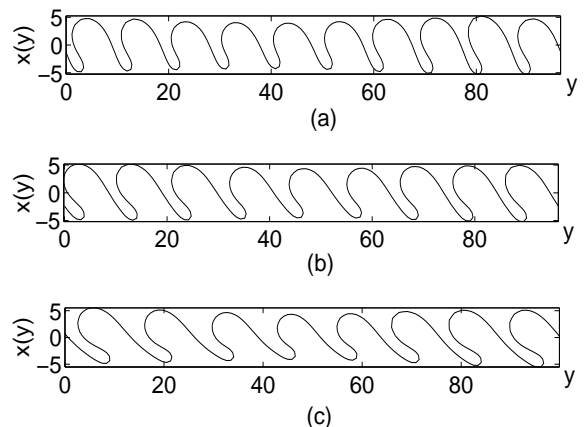


FIG. 9: Comparison of the step evolution as the angle φ increases: (a) $t = 230$, $\varphi = \pi/6$; (b) $t = 330$, $\varphi = \pi/4$; (c) $t = 640$, $\varphi = \pi/3$.

In Fig. 8, we show configurations of the system with $\varphi = \pi/4$. Fig. 8 suggests that the linear instability is induced by the perpendicular component of the field. However, as the magnitude of the instability grows, the peaks turn gradually until they are aligned with the direction of the field. We see the same peak turning process when the angle φ is varied while keeping f constant. However, since the perpendicular component decreases with increasing φ , both the wavelength selected by the initial instability as in Eq. (11) and the time period before it forms increases monotonically with φ . The numerical results for three particular angles are shown in Fig. 9.

To provide a more qualitative understanding of the pattern formation process, we neglect the higher order terms in κ in Eq. (22). To linear order in κ , Eq. (22) becomes

$$\frac{v_n}{\Omega D_s c_s^0} = f \kappa \cos(\varphi - \theta) - f \sin(\varphi - \theta) \partial_\tau \kappa + \Gamma \partial_\tau^2 \kappa. \quad (23)$$

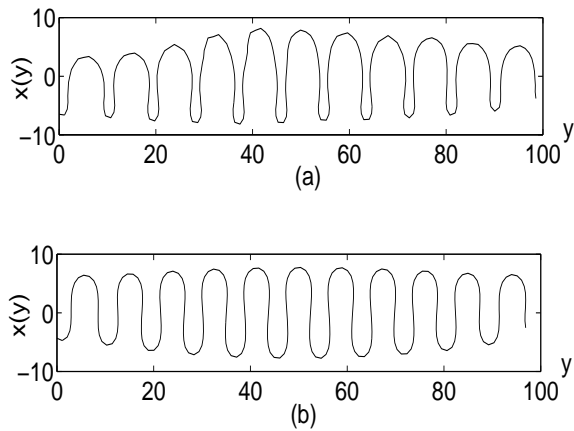


FIG. 10: A study of the asymmetry of the cellular patterns: (a) $t = 180$, a snapshot of the system given by Eq. (24). Note the close agreement with Fig. 7(c). This shows that the simplified Eq. (23) with only terms linear in κ captures most features of Eq. (22); (b) $t = 180$, a snapshot of a model equation where the term $\sim \partial_\tau \kappa$ is left out of Eq. (24). Clearly this term is mainly responsible for the asymmetric shape in (a).

In particular, for $\varphi = 0$

$$\frac{v_n}{\Omega D_s c_s^0} = f \kappa \cos \theta + f \sin \theta \partial_\tau \kappa + \partial_\tau^2 \kappa. \quad (24)$$

In the usual Mullins-Sekerka instability κ alone appears in the first term. Here however we have $\kappa \cos \theta$, resulting from field driven diffusion inside the step region. The extra $\cos \theta$ term brings in a field induced anisotropy that makes the peaks and valleys of a perturbation preferably grow rather than the sides. This stabilizes cellular structures. This anisotropy will keep the tip unsplit, and it provides a cut off as the sides become nearly vertical. Thus the cellular shapes formed under the influence of the external field do not emit side branches, in contrast to most systems that undergo a Mullins-Sekerka instability.

The second term in Eq. (23) is a flux induced by $-\kappa$ that effectively transports mass from the bottom to the top of a bulge and is responsible for the asymmetric shape of the peaks and valleys, as is illustrated in Fig. 10.

Although Eq. (23) is linear in the curvature, κ itself is a highly nonlinear function of the deviation from a straight step. The early evolution is governed by the following linearized equation

$$\frac{1}{\Omega D_s c_s^0} \frac{\partial x}{\partial t} = -f \cos \varphi \frac{\partial^2 x}{\partial y^2} - f \sin \varphi \frac{\partial^3 x}{\partial y^3} - \Gamma \frac{\partial^4 x}{\partial y^4}. \quad (25)$$

The above equation is unstable when $f \cos \varphi > 0$, suggesting that the wavelength selection is determined by the perpendicular component of the field. For $\varphi = 0$, perturbations with wavenumber $q_0 = 1/(\sqrt{2}\xi)$ are maximally amplified. For $0 < \varphi < \pi/2$, the most unstable wavenumber selected by the linear instability is decreased by a factor of $\sqrt{\cos \varphi}$, i.e., $q_\varphi = q_0 \sqrt{\cos \varphi}$.

As the instability grows, the field induced anisotropy characterized by the factor $\cos(\varphi - \theta)$ becomes more significant. As in the $\varphi = 0$ case above, the anisotropy makes the initial sinusoidal wave grows preferably in the direction where $\cos(\varphi - \theta)$ in Eq. (23) attains its minimum. Thus the wave will be continuously distorted until the peaks point toward the field direction, and subsequently only the magnitude of the pattern grows.

VIII. CONCLUSION

In this paper we have studied a physically suggestive two-region diffusion model. The basic idea is to consider different hopping rates associated with different reconstruction and bonding in the terrace and step regions. The resulting steady state profiles provide important insight into the physical origins of both step bunching and wandering instabilities. Step bunching is induced by positive chemical potential gradients on terraces that are essentially determined by the sign of $f(R - 1)$. We argue that step wandering in Si(111) does not arise from the well known Mullins-Sekerka instability. Rather, it is induced by driven diffusion along the step edge under the influence of a step-down force, and only becomes significant when step bunching is absent, which requires a negative kinetic coefficient.

We also carried out a mapping from the two-region model to a sharp step model using a simple extrapolation procedure. The result connects the kinetic coefficients in sharp step models to relative diffusion rates in terrace and step regions. In particular, the lowest order result shows that the kinetic coefficients are independent of the driving field, in contrast to earlier suggestions.²⁰

A coherent scenario for Si(111) electromigration is proposed based on the stability analysis of the model. In particular, the mysterious second temperature regime is interpreted using a negative kinetic coefficient. This allows the step wandering that generally occurs with a step-down force to be separated from step bunching. The transition between different temperature regimes is governed by the relative diffusivity in the terrace and step regions. Other theories can predict a reversal of step bunching arising from a change in step transparency^{17,18} or from a change of sign of the effective charge.³⁸ However, neither approach can give a consistent treatment for step wandering.

The long time evolution of the step instabilities was calculated by numerical integration of a set of equations based on the standard velocity function formalism with the addition of a periphery diffusion term. The linear instabilities are recovered at short times and interesting 2D pattern formation is seen at longer times in qualitative agreement with experiment.

We also showed that a geometric representation of the step provides a simple way to describe the nonlinear evolution of step wandering patterns with large curvatures. The resulting cellular patterns when the driving field is at

an angle to the step shows significant step “overhangs”, which can not be captured by standard multi-scale expansion methods.^{39,40}

The two-region model can also be modified to explain many features of the very different step bunching behavior seen on Si(001) surfaces.²² Thus it provides a simple and unified perspective that can shed light on both general properties of current-induced step bunching and wandering instabilities and their specific manifestations on Si surfaces.

Acknowledgments

We are especially grateful to Daniel Kandel for many stimulating discussions on connecting the two-region model to sharp step models. We also thank Ted Einstein, Oliver Pierre-Louis, and Ellen Williams for helpful comments. This work has been supported by the NSF-MRSEC at the University of Maryland under Grant No. DMR 00-80008.

APPENDIX: LINEAR STABILITY ANALYSIS IN A SHARP INTERFACE MODEL

A complete 2D stability analysis in a generalized BCF model is performed in this section, with boundary conditions dictated by mapping from the two-region model. Using the quasi-stationary approximation, we first solve for the static concentration field c_t on the terrace as given by

$$D_t \nabla^2 c_t - \frac{D_t \mathbf{F}}{k_B T} \cdot \nabla c_t = 0, \quad (\text{A.1})$$

subject to the general linear kinetics boundary condition at the sharp step:

$$\pm D_t [\nabla c_t - f c_t]_{\pm} \cdot \hat{n} = k [c_t - c_{eq}^0 (1 + \Gamma \kappa)]_{\pm}. \quad (\text{A.2})$$

Here κ is the curvature, defined to be positive for a circle. The normal step velocity is determined by balancing the fluxes locally at the step

$$v_n \Delta c = \hat{n} \cdot [\mathbf{J}_t^- - \mathbf{J}_t^+] - \partial_{\tau} J_s. \quad (\text{A.3})$$

Here J_s is the periphery flux of the mobile atoms along the interface, which can be viewed as the coarse-grained contribution from the parallel diffusion in the two-region model. In general, J_s takes the form

$$J_s = -D_s \partial_{\tau} c_s + D_s \frac{\mathbf{F} \cdot \hat{\tau}}{k_B T} c_s, \quad (\text{A.4})$$

where $c_s \simeq c_{eq}^0 s$ gives the effective number of ledge atoms per unit step length.

Consider a 2D perturbation on the step profile in the form $\delta x_n(y, t) \equiv x_n(y, t) - x_n^0 = \varepsilon_n e^{\omega t + i q y} + c.c.$, where x_n^0 is the step position for 1D steady state and ε_n is the 1D perturbation previously defined. In general ω can be complex, i.e. $\omega = \omega_r + i \omega_i$, but we are only interested in the real part ω_r whose sign determines the instability. The calculation follows standard methods, and the result can cast in the familiar Bales and Zangwill’s form²⁵:

$$\omega_r = -\Gamma q^2 h(q, f, \phi) + f g(q, f, \phi). \quad (\text{A.5})$$

Here the stabilizing piece $h(q, f, \phi)$ is given by

$$\begin{aligned} \frac{h(q, f, \phi)}{\Omega D_t c_{eq}^0} &= \frac{2\lambda [\cosh(\lambda l) - \cos \phi \cosh(fl/2)] + 2dq^2 \sinh(\lambda l)}{\mathcal{D}} \\ &+ \frac{a}{R} q^2, \end{aligned} \quad (\text{A.6})$$

and the destabilizing piece $g(q, f, \phi)$ is

$$\begin{aligned} \frac{g(q, f, \phi)}{\Omega D_t c_{eq}^0} &= \frac{2df}{[df(e^{fl} + 1) + e^{fl} - 1] \mathcal{D}} \\ &\times \{ 2\lambda [\cosh(\lambda l) - e^{fl/2} \cos \phi] \\ &+ 2dq^2 e^{fl/2} \cosh(fl/2) \sinh(\lambda l) \\ &+ \sinh(fl/2) (\Lambda_+ e^{\Lambda_- l} - \Lambda_- e^{\Lambda_+ l}) \} \\ &+ \frac{a}{R} q^2, \end{aligned} \quad (\text{A.7})$$

where

$$\mathcal{D} = 2d\lambda \cosh(\lambda l) + (1 + d^2 q^2) \sinh(\lambda l), \quad (\text{A.8})$$

$\lambda = \sqrt{f^2 + 4q^2}/2$ and $\Lambda_{\pm} = f/2 \pm \lambda$.

It is easy to see that $h(q, f, \phi)$ is positive definite; thus the first term in Eq.(A.5) is always stabilizing. In particular, we obtain the results for the equilibrium relaxation by taking the limit $f \rightarrow 0$

$$\begin{aligned} \frac{\omega_0(q, \phi)}{\Omega D_t c_{eq}^0} &= -\Gamma q^2 \left\{ \frac{2q [\cosh(q l) - \cos \phi + dq \sinh(q l)]}{2dq \cosh(q l) + (1 + d^2 q^2) \sinh(q l)} \right. \\ &\left. + \frac{s}{R} q^2 \right\}. \end{aligned} \quad (\text{A.9})$$

The two terms in the curly brackets account for relaxation through terrace diffusion and periphery diffusion respectively. The second term in Eq. (A.5) is completely driven by the field, and it vanishes identically as $f \rightarrow 0$ since $\lim_{f \rightarrow 0} g(q, f, \phi)$ is finite.

For current-induced instabilities that are of interest of this paper, we can take the weak field ($fl \ll 1$) and long wavelength ($ql \ll 1$) limit. In this limit, the stability functions to linear order in the field are given in Eqs. (14)-(16).

-
- ¹ A. V. Latyshev, A. L. Aseev, A. B. Krasilnikov, and S. I. Stenin, *Surf. Sci.* **213**, 157 (1989).
- ² Y. Homma, R. McClelland, and H. Hibino, *Jpn. J. Appl. Phys.* **29**, L2254 (1990).
- ³ H. Yamaguchi and K. Yagi, *Surf. Sci.* **287/288**, 820 (1993).
- ⁴ E. D. Williams, E. S. Fu, Y.-N. Yang, D. Kandel, and J. D. Weeks, *Surf. Sci.* **336**, L746 (1995).
- ⁵ Y.-N. Yang, E. S. Fu, and E. D. Williams, *Surf. Sci.* **356**, 101 (1996).
- ⁶ Y. Homma and N. Aizawa, *Phys. Rev. B* **62**, 8323 (2000).
- ⁷ M. Degawa, H. Minoda, Y. Tanishiro, and K. Yagi, *Surf. Rev. Lett.* **6**, 977 (1999).
- ⁸ M. Degawa, H. Nishimura, Y. Tanishiro, H. Minoda, and K. Yagi, *Jpn. J. Appl. Phys.* **38**, L308 (1999).
- ⁹ M. Degawa, K. Thürmer, I. Morishima, H. Minoda, K. Yagi, E. D. Williams, *Surf. Sci.* **487**, 171 (2001).
- ¹⁰ M. Degawa, H. Minoda, Y. Tanishiro, and K. Yagi, *Phys. Rev. B* **63**, 045309 (2001).
- ¹¹ S. Stoyanov, *Jpn. J. Appl. Phys., Part 1* **30**, 1 (1991).
- ¹² E. S. Fu, D.-J. Liu, M. D. Johnson, J. D. Weeks, and E. D. Williams, *Surf. Sci.* **385**, 259 (1997).
- ¹³ W. K. Burton, N. Cabrera, and F. C. Frank, *Proc. R. Soc. London, A* **243**, 299 (1951).
- ¹⁴ G. Ehrlich and F. Hudda, *J. Chem. Phys.* **44**, 1039 (1966).
- ¹⁵ R. L. Schwoebel and E. J. Shipsey, *J. Appl. Phys.* **37**, 3682 (1966).
- ¹⁶ O. Pierre-Louis, M. R. D'Orsogna, and T. L. Einstein, *Phys. Rev. Lett.* **82**, 3661 (1999).
- ¹⁷ S. Stoyanov, *Surf. Sci.* **416**, 200 (1998).
- ¹⁸ M. Sato, M. Uwaha, and Y. Saito, *Phys. Rev. B* **62**, 8452 (2000).
- ¹⁹ M. Sato, M. Uwaha, Y. Saito, and Y. Hirose, *Phys. Rev. B* **65**, 245427 (2002).
- ²⁰ N. Suga, J. Kimpara, N.-J. Wu, H. Yasunaga, and A. Natori, *Jpn. J. Appl. Phys.* **39**, 4412 (2000).
- ²¹ A preliminary account of some these ideas is given in T. Zhao, J. D. Weeks, and D. Kandel, submitted.
- ²² T. Zhao, J. D. Weeks, and D. Kandel, submitted.
- ²³ D.-J. Liu, and J. D. Weeks, *Phys. Rev. B* **57**, 14891 (1998).
- ²⁴ See, e.g., K. Thürmer, D. J. Liu, E. D. Williams, and J. D. Weeks, *Phys. Rev. Lett.* **83**, 5531 (1999) for experimental parameter values.
- ²⁵ G. S. Bales, and A. Zangwill, *Phys. Rev. B* **41**, 5500 (1990).
- ²⁶ W. W. Mullins and R. F. Sekerka, *J. Appl. Phys.* **34**, 323 (1963).
- ²⁷ W. W. Mullins and R. F. Sekerka, *J. Appl. Phys.* **35**, 444 (1964).
- ²⁸ See, e.g., K. Binder and P. C. Hohenberg, *Phys. Rev. B* **6**, 3461 (1972).
- ²⁹ P. Politi, and J. Villain, *Phys. Rev. B* **54**, 5114 (1996).
- ³⁰ S. D. Cohen, R. D. Schroll, T. L. Einstein, J.-J. Métois, H. Gebremariam, H. L. Richards, E. D. Williams, *Phys. Rev. B* **66**, 115310 (2002).
- ³¹ P. Bennema and G. H. Gilmer, in *Crystal Growth: An Introduction*, edited by P. Hartman, p.263 (North Holland, Amsterdam, 1973).
- ³² D.-J. Liu, J. D. Weeks, and D. Kandel, *Surf. Rev. Lett.* **4**, 107 (1997).
- ³³ J. D. Weeks, D.-J. Liu, H.-C. Jeong, *Dynamics of crystal surfaces and interfaces* edited by P. Duxbury and T. Spence (Plenum, New York), pp. 199-216 (1997).
- ³⁴ See, e.g., D.-J. Liu, E. S. Fu, M. D. Johnson, J. D. Weeks, and E. D. Williams, *J. Vac. Sci. Tech. B* **14**(4), 2799 (1996).
- ³⁵ R. C. Brower, D. A. Kessler, J. Koplik, and H. Levine, *Phys. Rev. Lett.* **51**, 1111 (1983).
- ³⁶ R. C. Brower, D. A. Kessler, J. Koplik, and H. Levine, *Phys. Rev. A* **29**, 1335 (1984).
- ³⁷ J. D. Weeks, and W. van Saarloos, *Phys. Rev. A* **35**, 3001 (1987).
- ³⁸ D. Kandel and E. Kaxiras, *Phys. Rev. Lett.* **76**, 1114 (1996).
- ³⁹ I. Bena, C. Misbah, and A. Valance, *Phys. Rev. B* **47**, 7408 (1993).
- ⁴⁰ O. Pierre-Louis, C. Misbah, Y. Saito, J. Krug, P. Politi, *Phys. Rev. Lett.* **80**, 4221 (1998).